Geochimica et Cosmochimica Acta, Vol. 69, No. 8, pp. 2133–2140, 2005

0016-7037/05 $30.00 + .00

doi:10.1016/j.gca.2004.10.018

Thermochemistry of yavapaiite $KFe(SO_4)_2$: formation and decomposition

Ferenc Lázár Forray, Christophe Drouet† and Alexandra Navrotsky*
Thermochemistry Facility and NEAT ORU, University of California at Davis, One Shields Avenue, Davis, CA 95616, USA

(*Received June* 1, 2004; *accepted in revised form October* 27, 2004)

Abstract—Yavapaiite, $KFe(SO_4)_2$, is a rare mineral in nature, but its structure is considered as a reference for many synthetic compounds in the alum supergroup. Several authors mention the formation of yavapaiite by heating potassium jarosite above ca. 400°C. To understand the thermal decomposition of jarosite, thermodynamic data for phases in the K-Fe-S-O-(H) system, including yavapaiite, are needed. A synthetic sample of yavapaiite was characterized in this work by X-ray diffraction (XRD), scanning electron microscopy (SEM), Fourier transform infrared spectroscopy (FTIR), and thermal analysis. Based on X-ray diffraction pattern refinement, the unit cell dimensions for this sample were found to be a = 8.152 ± 0.001 Å, b = 5.151 ± 0.001 Å, c = 7.875 ± 0.001 Å, and β = 94.80°. Thermal decomposition indicates that the final breakdown of the yavapaiite structure takes place at 700°C (first major endothermic peak), but the decomposition starts earlier, around 500°C. The enthalpy of formation from the elements of yavapaiite, $KFe(SO_4)_2$, $\Delta H°_f = -2042.8 \pm 6.2$ kJ/mol, was determined by high-temperature oxide melt solution calorimetry. Using literature data for hematite, corundum, and Fe/Al sulfates, the standard entropy and Gibbs free energy of formation of yavapaiite at 25°C (298 K) were calculated as $S°(\text{yavapaiite}) = 224.7 \pm 2.0$ J.mol^{-1}.K^{-1} and $\Delta G°_f = -1818.8 \pm 6.4$ kJ/mol. The equilibrium decomposition curve for the reaction jarosite = yavapaiite + Fe_2O_3 + H_2O has been calculated, at pH_2O = 1 atm, the phase boundary lies at 219 ± 2°C. *Copyright © 2005 Elsevier Ltd*

1. INTRODUCTION

Yavapaiite is a mineral corresponding to the chemical formula $KFe(SO_4)_2$ (monoclinic, space group C2/m). Its existence was first reported by Hutton (1959). The sample analyzed then had been collected earlier, in 1941, in the copper mining center of Jerome, Arizona. Hutton underlines the very limited occurrence of yavapaiite on that site. Similarly, very few reports of natural occurrence of this compound are available (Hutton, 1959; Volchanova et al., 1974).

In addition to anhydrous yavapaiite, two hydrated forms have been observed: the monohydrate $KFe(SO_4)_2 \cdot H_2O$, krausite, and the tetrahydrate $KFe(SO_4)_2 \cdot 4H_2O$, goldichite. Krausite was first documented by Foshag (1931) in a geological study in the Calico Hills, California. Goldichite (in San Rafael Swell, Utah) was only reported decades later by Rosenzweig and Gross (1955). The crystal structures of both hydrates have been investigated in several studies (Foshag, 1931; Rosenzweig and Gross, 1955; Hutton, 1959; Graeber et al., 1965; Graeber and Rosenzweig, 1971; Effenberger et al., 1986; Florencia et al., 1995). Although, like yavapaiite, krausite and goldichite crystallize in the monoclinic system, their space groups are different from that of yavapaiite: $P2_1/m$ and $P2_1/c$ respectively. This suggests that the atomic arrangements of the hydrates differ significantly from that of (anhydrous) yavapaiite. Therefore, the preparation of yavapaiite by dehydration of the hydrates through heating is likely to be problematic, and this might be the origin of the unsuccessful attempts reported by Hutton (1959).

Although synthetic yavapaiite has been prepared, details on its synthesis protocol are seldom given. Among the information available, Hutton (1959) mentions the "vacuum crystallization of a solution containing K_2SO_4 and $Fe_2(SO_4)_3$ in a 1:1 mol/L ratio and subsequent heat treatment of the crystallized product at 400°C." Yavapaiite can also be formed by heating jarosite species above ca. 400°C, through a process of dehydroxylation (Kulp and Adler, 1950; Kubisz, 1971; Arno, 1984; Drouet and Navrotsky, 2003). The corresponding chemical reaction is the following:

$$KFe_3(SO_4)_2(OH)_6 \rightarrow KFe(SO_4)_2 + Fe_2O_3 + 3H_2O \quad (1)$$

To date, published results on yavapaiite (Hutton, 1959; Graeber and Rosenzweig, 1971; Anthony et al., 1972; Giester, 1993) only deal with crystal structure and physical properties such as color, cleavage and fracture, and optical features. From a structural point of view, yavapaiite is often considered as a reference in the alum supergroup $M^+M^{3+}(XO_4)_2$. Other compounds from this supergroup are selenates like $KMn(SeO_4)_2$ (Giester, 1995) and $NaFe(SeO_4)_2$ (Giester, 1993; Giester, 1995), and phosphates such as $BaMo(PO_4)_2$ (Leclaire et al., 1995), Ba(Hf,Zr)$(PO_4)_2$ (Miao and Torardi, 2000). Also, yavapaiite is a triangular-lattice magnet often used as a model in magnetic studies of alum-like structures (Bramwell et al., 1996).

However, to our knowledge, no information is available on the thermodynamics of this phase. Despite the relative rarity of yavapaiite, thermodynamic data are needed for the establishment of phase diagrams for the K-Fe-S-O-(H) system, often encountered in geological and environmental issues such as acid mine drainage and weathering of sulfide ore deposits. A couple of indirect observations of the surface of Mars indicate that jarosite could be present (Burns, 1987; Morris and Golden, 1998). The very recent discovery of jarosite as a significant phase on Mars (Klingelhöfer, 2004), makes yavapaiite, a dehydratation product of jarosite, important in limiting the stability of jarosite in an increasingly dry environment.

* Author to whom correspondence should be addressed (anavrotsky@ucdavis.edu).
† *Present address:* CIRIMAT/ENSIACET, UMR CNRS 5085, Physico-Chimie des Phosphates, 118 route de Narbonne, 31077 Toulouse Cedex 04, France.

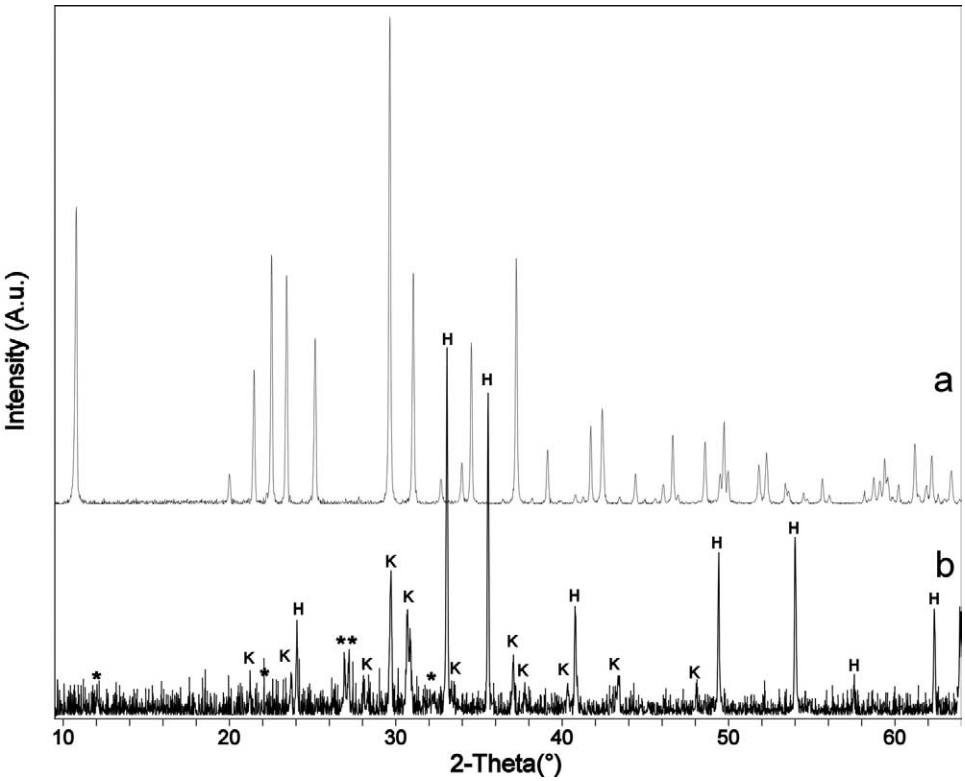

Fig. 1. X-ray diffraction pattern for the yavapaiite sample (a) and after heat treatment at 1000°C (b). H—hematite; K—K_2SO_4 (arcanite); *—unidentified.

In this paper, we report for the first time the enthalpy of formation, from the oxides and elements, of yavapaiite as determined by high-temperature oxide melt calorimetry. Then, the standard entropy and Gibbs free energy of formation of yavapaiite are evaluated.

2. MATERIALS AND METHODS

2.1. Sample Synthesis

The synthesis protocol used in this work was strongly inspired from data reported in ICDD-PDF file 29-1438. Successful synthesis of yavapaiite was based on the following reaction:

$$KOH + FeOOH + 2H_2SO_4 \rightarrow KFe(SO_4)_2 + 3H_2O \quad (2)$$

For this reaction, we used high purity ACS-certified reagents KOH, FeOOH (goethite), H_2SO_4, and ethanol from Alfa Aesar and Fisher. 0.35 g KOH was dissolved, under ultrasonics, in 25 mL deionized water, and 0.56 g FeOOH in 50 mL deionized water, and the two solutions were mixed under ultrasonics for 20 min. To the solution obtained, 1.23 g H_2SO_4 and 25 mL deionized water were added and mixed under ultrasonics for another 20 min. The solution was placed in a beaker and stirred continuously using a magnetic bar. To this solution, 100 mL of ethanol were gradually added and the solution was stirred for 24 h. The resulting solution was heated to 70°C under continuous stirring, until the viscosity clearly increased and the magnet slowed. We continued to heat the solution at 70°C without stirring to complete evaporation of the solvent.

The resulting pale pink powder was placed in a desiccator at 115°C for 24 h., and heat-treated in air at 200°C for 7 days.

2.2. Characterization

Powder X-ray diffraction (XRD) was run on a Scintag PAD-V diffractometer operated at 45 kV and 40 mA using CuK_α radiation (λ = 1.54056 Å). Before the experiments, the diffractometer was calibrated with quartz. Unit cell parameters were derived by Rietveld refinement using the Jade program (Materials Data Inc., 2001). The samples were run in step-scan mode, with steps of 0.02 and dwell time 2.5 s.

The synthesized yavapaiite was investigated using a FEI XL30-SFEG high-resolution scanning electron microscope (SEM) coupled with an EDAX Phoenix EDS system. The powder sample was placed on an aluminum sample holder and coated with carbon.

Fourier transform infrared (FTIR) spectra were recorded with a Bruker EQUINOX 55 spectrometer. Approximately 1 mg of sample was mixed with 150 mg KBr. The powder was pressed into a 13-mm pellet. A blank KBr pellet was prepared for background correction. To avoid contamination, the infrared spectra were recorded immediately after pellet preparation, and the spectrometer was flushed continuously with nitrogen. Spectra were collected in the 400–4000 cm^{-1} range, with a resolution of 4 cm^{-1}. Baseline correction was made before interpretation of the spectra.

The thermal decomposition of yavapaiite was investigated from room temperature to 1000°C using a Netzsch STA 449. Thermogravimetry (TG) and differential scanning calorimetry (DSC) analyses were carried out at by heating at 10°C/min and under flushing oxygen at 50 mL/min.

2.3. High-Temperature Calorimetry

High-temperature oxide melt calorimetry was carried out at 700°C in a custom built Tian-Calvet twin calorimeter described earlier by Navrotsky (1977; 1997), with sodium molybdate $3Na_2O \cdot 4MoO_3$ as solvent. Solution calorimetry converts products and reactants to the same final state: a dilute solution of oxides dissolved in the oxide melt. Pellets of 5 mg of the sample are dropped into a platinum crucible containing the solvent, located in the hot zone of the calorimeter. During the experiments, oxygen was flushed above the melt (~40 mL/min) and bubbled through the solvent (~7 mL/min) to maintain oxidizing conditions and stir the melt.

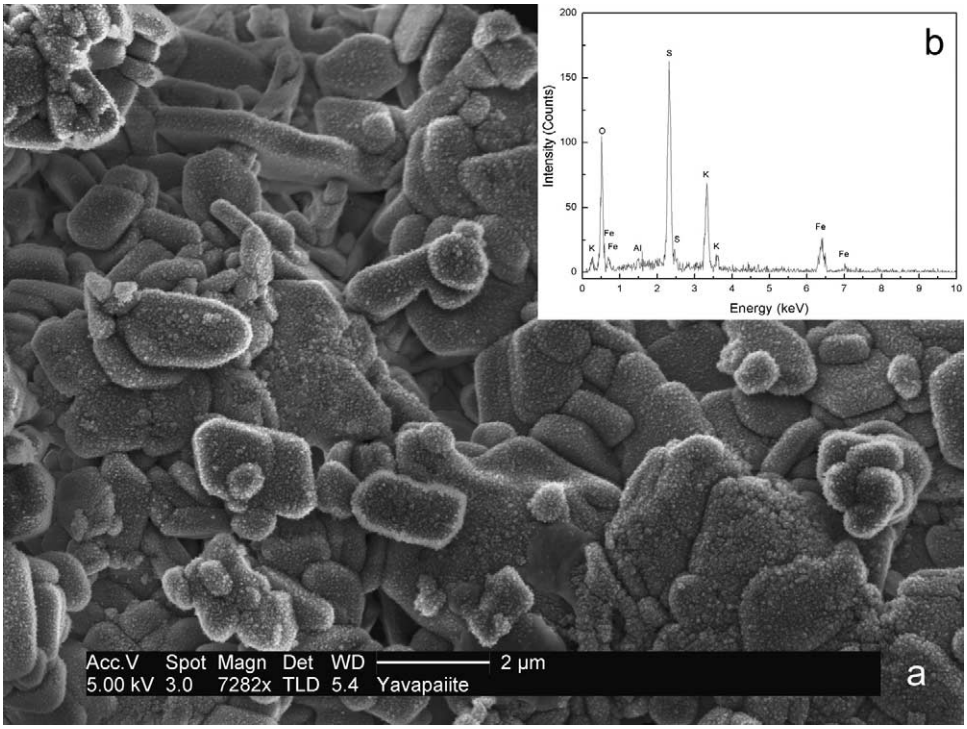

Fig. 2. SEM image and EDS spectra of the yavapaiite sample.

The measured heat effect, or enthalpy of drop solution (ΔH_{ds}), is the sum of the heat content of the sample, its heat of solution, and the heat related to gas release. The enthalpy of formation of a given compound can be determined from ΔH_{ds} through the use of an appropriate thermodynamic cycle. We have shown in recent studies (Majzlan et al., 2002; Drouet and Navrotsky, 2003) that sulfates dissolve in $3Na_2O \cdot 4MoO_3$, with all the sulfate remaining in the melt. The water is evolved into the gas phase and removed from the calorimeter (Navrotsky et al., 1994).

3. RESULTS AND DISCUSSIONS

3.1. Characterization

The X-ray diffraction pattern obtained (Fig. 1) is similar to that of yavapaiite described in ICDD-PDF file 61-0998. No other crystalline phases were detected. This pattern was indexed in the C2/m space group, and all reflections with relative intensities ≥2% were seen. The unit cell parameters are a = 8.152 ± 0.001 Å, b = 5.151 ± 0.001 Å, c = 7.875 ± 0.001 Å, and β = 94.80°. These values are close to those a = 8.152(5)Å, b = 5.153(4)Å, c = 7.877(5)Å and β = 94.90° reported by Graeber and Rosenzweig (1971) for yavapaiite from Jerome, Arizona, and they also agree with reference data (ICDD-PDF files 29-1438, 73-0288, and 74-0384). In contrast, the unit cell parameters given by Anthony (1972) and Hutton (1959) are slightly different from ours.

The X-ray diffraction pattern (Fig. 1) for yavapaiite heated to 1000°C in air shows the presence of two main phases, hematite Fe_2O_3 (ICDD-PDF 60-8558) and arcanite K_2SO_4 (ICDD-PDF 64-3139). However, some unidentified peaks are also observed, indicating the presence of other decomposition products.

Observation of the sample by SEM (Fig. 2) shows well developed crystals ranging in size from 250 nm to 5 μm. The morphology of the crystals, namely the forms {001}, {100} and, {110} is roughly comparable to that described by Hutton (1959). The EDS spectra performed on these crystals show the presence of K, Fe, S, O and the absence of impurities (Fig. 2).

The FTIR spectrum is shown in Figure 3. To our knowledge, there are no FTIR references for this compound in the literature. The spectrum shows a weak hump in the 2900–3700 cm^{-1} region. The presence of this absorption is typical for O-H stretching, which would indicate the presence of some water molecules either within the structure or as adsorbed species. However, the low intensity of this band and the absence of a sharp absorption band around 1630 cm^{-1}, indicative of O-H bending, suggests that the amount of water involved is very limited. This is confirmed by the agreement between the XRD pattern obtained on our sample and reference data, and in particular by the absence of peaks assignable to krausite or goldichite.

Several absorption bands are observed in the 800–1300 cm^{-1} region (Fig. 3), namely at 1249, 1089, 1050, and 1026 cm^{-1}. In the case of Na_2SO_4, Smith (1999) reported the presence of a band at 1134 cm^{-1} that was assigned to SO_4 stretching. Also, in the case of jarosites, the SO_4 stretching vibrations ν_3(doublet) and ν_1 appear close to 1190, 1090 and 1005 cm^{-1} respectively (Arkhipenko et al., 1987, Drouet and Navrotsky, 2003). It is therefore likely that the bands observed here at 1249 and 1089 cm^{-1} could be attributed to vibration mode ν_3. A set of absorption bands is also observed at lower frequencies, in the range 400–700 cm^{-1}, at 445, 471, 591, 621, and 682 cm^{-1} (Fig. 3). However, due to the complexity of the spectrum in this region, and the lack of FTIR data on similar compounds, it is difficult to interpret unequivocally these bands without additional work, which was beyond the scope of this study.

TG/DSC shows two intense endothermic peaks and a series

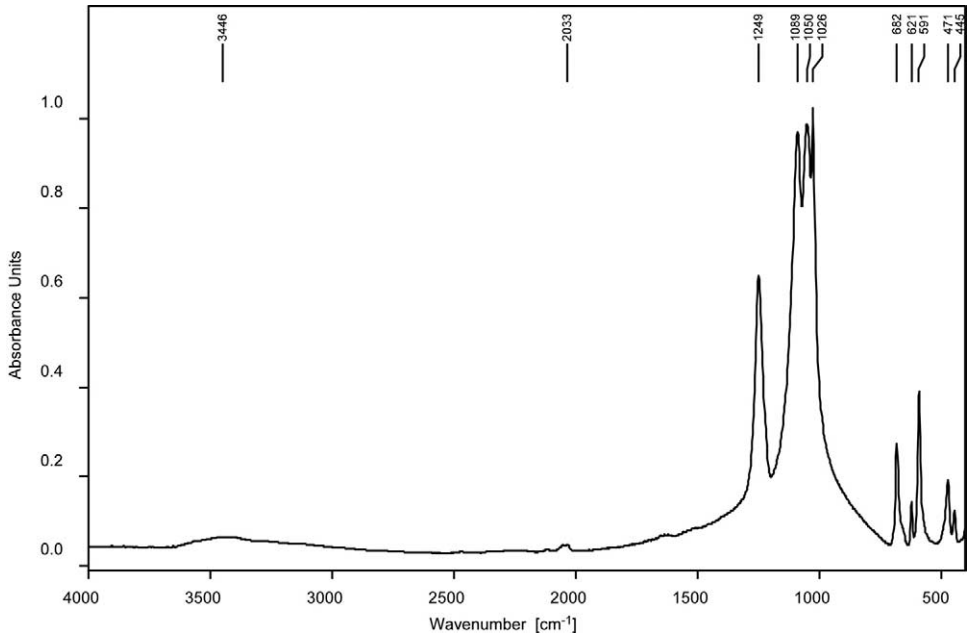

Fig. 3. FTIR spectra of the yavapaiite.

of weaker endotherms and exotherms (Fig. 4). In general terms, yavapaiite decomposition can be summarized by the following reaction:

$$2KFe(SO_4)_2 \rightarrow K_2SO_4 + Fe_2O_3 + 3SO_3 \quad (3)$$

However, this reaction only indicates the overall stoichiometry, and the actual decomposition process appears to be more complex. As shown by the TG/DSC curves (Fig. 4), several steps are involved during the decomposition, and intermediate phases alternatively form and decompose. The color change from pale pink to brown or red-brown, as observed during sample treatment in the temperature range 350 to 400 °C, can be attributed to the decomposition of yavapaiite and formation of hematite.

Such color changes are documented in the literature. Hutton (1959) mentioned that the X-ray diffraction pattern of yavapaiite heat-treated at 280 and 400°C for 17 and 8 hours respectively showed no differences from the unheated sample. This author also mentioned that, if yavapaiite is heated to 500°C, its color changes to pale brown, and that for higher temperatures the color turns to red-brown. From the study of the decomposition of $KFeS_2$ under an oxidative atmosphere, Furtado et al. (1989) concluded that the yavapaiite formed during the decom-

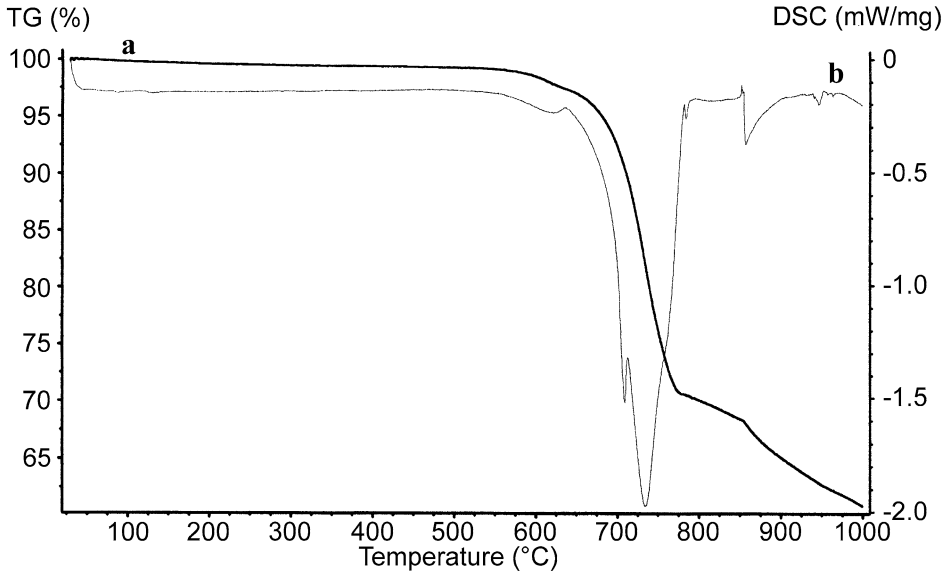

Fig. 4. TG (a) and DSC (b) curves for yavapaiite heated in air up to 1000°C.

Table 1. Thermodynamic cycle used for the determination of ΔH_f^o of yavapaiite.

Reaction[a]	$\Delta H_{reaction}$
(1) $KFe(SO_4)_2$ (s, 298) → 1/2 K_2O (soln, 973) + 1/2 Fe_2O_3 (soln, 973) + 2 SO_3 (soln, 973)	ΔH_{ds} (yavapaiite)
(2) α-Fe_2O_3 (s, 298) → Fe_2O_3 (soln, 973)	ΔH_{ds} (α-Fe_2O_3)
(3) 2 Fe (s, 298) + 3/2 O_2 (g, 298) → α-Fe_2O_3 (s, 298)	ΔH_f^o (α-Fe_2O_3)
(4) K_2SO_4 (s, 298) → K_2O (soln, 973) + SO_3 (soln, 973)	ΔH_{ds} (K_2SO_4)
(5) 2 K (s, 298) + S (s, 298) + 2 O_2 (g, 298) → K_2SO_4 (s, 298)	ΔH_f^o (K_2SO_4)
(6) SO_3 (g, 298) → SO_3 (soln, 973)	ΔH_{ds} ($SO_{3(g)}$)[b]
(7) S (s, 298) + 3/2 O_2 (g, 298) → SO_3 (g, 298)	ΔH_f^o (SO_3)
Formation of yavapaiite:	
K (s, 298) + Fe (s, 298) + 2 S (s, 298) + 4 O_2 (g, 298) → $KFe(SO_4)_2$ (s, 298)	ΔH_f^o (yavapaiite)
ΔH_f^o (yavapaiite) = $-\Delta H_1$ + 1/2 ΔH_2 + 1/2 ΔH_3 + 1/2 ΔH_4 + 1/2 ΔH_5 + 3/2 ΔH_6 + 3/2 ΔH_7	

[a] "s", "g" and "soln" are for "solid", "gas" and "in solution" (in sodium molybdate) respectively.
[b] Majzlan et al. (2002).

position process was stable only in the 400 to 450 °C temperature range. Also, several authors (Kulp and Adler, 1950; Kubisz, 1971; Drouet and Navrotsky, 2003) mentioned that yavapaiite can form by heating jarosite above 400°C. Indeed, heated to 550°C, jarosite was found to decompose, forming hematite and yavapaiite (Arno, 1984).

Most authors found that the decomposition of yavapaiite takes place near 700°C (Kulp and Adler, 1950; Kubisz, 1971; Drouet and Navrotsky, 2003). Our study indicates that the final breakdown of the yavapaiite structure takes place at 700°C (first main endotherm), but that the decomposition starts earlier, around 500°C. The second endothermic peak, at 856°C, can be attributed to decomposition of some intermediate product. Kubisz (1971) reported in the case of jarosite decomposition that SO_3 can remain in the system even at 1000°C. The decomposition of the K_2SO_4 takes place only above 1000°C (at 1069°C, Kubisz, 1971).

The breakdown of the crystal structure takes place slowly at lower temperature (500°C), as the changes in yavapaiite color indicate. However, crystal size and differences in the heating process can also influence the temperature range where thermal decomposition of yavapaiite occurs, presumably by affecting the kinetics. Furthermore, see thermodynamic discussions below, the equilibrium decomposition temperature depend on the partial pressure of sulfur gases (SO_2, SO_3) above the sample. This in turn depends on how rapidly such gases are removed from the system as they are produced.

3.2. Thermodynamic Data

The heat of formation of yavapaiite was determined by high-temperature calorimetry using the thermodynamic cycle given in Table 1. This cycle involves the enthalpy of drop solution of yavapaiite (measured in this work) as well as that of hematite, potassium sulfate and sulfur trioxide, which were reported elsewhere (Majzlan et al., 2002; Drouet and Navrotsky, 2003). This cycle also uses the enthalpies of formation of these last three compounds (Robie and Hemingway, 1995). The corresponding numerical values are given in Table 2. Based on this cycle, the enthalpy of formation from the elements of yavapaiite was found to be $\Delta H^\circ_f = -2042.8 \pm 6.2$ kJ/mol. To our knowledge, this is the first experimental report for the heat of formation of this phase.

It is possible to estimate the standard entropy of yavapaiite by using solid-state equilibria involving this phase. One can, for example, consider the following reactions:

Table 2. Thermodynamic values used in this work.

Compound	ΔH_{ds}[a] (kJ/mol)	ΔH_f^o (kJ/mol)	S_f^o ($J.mol^{-1}.K^{-1}$)	ΔS_f^o ($J.mol^{-1}.K^{-1}$)	ΔG_f^o (kJ/mol)
$KFe(SO_4)_2$ (yavapaiite)	132.8 ± 1.5 (14)[a,b]	−2042.8 ± 6.2[a]	224.7 ± 5.0[a]	−751.8 ± 5.0[a]	−1818.8 ± 6.4[a]
α-Fe_2O_3 (hematite)	95.0 ± 1.8 (8)[b,c]	−826.2 ± 1.3[d]	87.4 ± 0.2[d]		
K_2SO_4	153.4 ± 1.8 (8)[b,c]	−1437.7 ± 0.5[d]	—		
$SO_{3(g)}$	−205.8 ± 3.7[b,e]	−395.7 ± 0.7[d]	—		
α-Al_2O_3 (corundum)	—	−1675.7 ± 1.3[d]	50.9 ± 0.1[d]		
$KAl(SO_4)_2$	—	−2470.9 ± 1.3[d]	204.6 ± 1.3[d]		
$Fe_2(SO_4)_3$	—	−2581.9 ± 2.9[d]	282.8 ± 2.9[d]		
$Al_2(SO_4)_3$	—	−3441.8 ± 1.8[d]	239.3 ± 1.2[d]		
K (s, 298)	—	0	64.67 ± 0.20[d]		
Fe (s, 298)	—	0	27.09 ± 0.13[d]		
S (s, 298)	—	0	32.05 ± 0.05[d]		
O_2 (g, 298)	—	0	205.15 ± 0.02[d]		

[a] This work
[b] Numbers in parentheses refer to the number of experiments performed. Uncertainties are two standard deviations of the mean.
[c] Drouet and Navrotsky (2003).
[d] Robie and Hemingway (1995).
[e] Majzlan et al. (2002).

$$2KFe(SO_4)_2 + Al_2O_3 \Leftrightarrow 2KAl(SO_4)_2 + Fe_2O_3 \quad (4)$$

and

$$2KFe(SO_4)_2 + Al_2(SO_4)_3 \Leftrightarrow 2KAl(SO_4)_2 + Fe_2(SO_4)_3 \quad (5)$$

Thermodynamic data for corundum (α-Al_2O_3), hematite (α-Fe_2O_3), iron (III) sulfate and aluminum sulfate are also given in Table 2. To a first approximation, one can assume that the change in entropy corresponding to such solid-state reactions is zero. In that case, the standard entropy of yavapaiite can be estimated from the equations:

$$S°(\text{yavapaiite}) \cong ½\,(2S°(KAl(SO_4)_2) + S°(Fe_2O_3) - S°(Al_2O_3)) \quad (6)$$

and

$$S°(\text{yavapaiite}) \cong ½\,(2S°KAl(SO_4)_2) + S°(Fe_2(SO_4)_3) - S°(Al_2(SO_4)_3)) \quad (7)$$

These reactions lead to the values 222.9 ± 1.3 J.mol^{-1}.K^{-1} and 226.4 ± 1.5 J.mol^{-1}.K^{-1} respectively. The average value S°(yavapaiite) = 224.7 ± 2.0 J.mol^{-1}.K^{-1} is a first approximation for the standard entropy of yavapaiite. Note however that this calculated uncertainty only takes into account the uncertainties on every term of Eqns. (6) and (7). One must bear in mind that the actual error on this value is probably higher due to the initial hypothesis that the entropy changes of Equilibria (4) and (5) are strictly zero. A more realistic error estimate would probably be of the order of ± 5 J.mol^{-1}.K^{-1} and this is used in further calculations.

Considering the enthalpy of formation and entropy discussed above for yavapaiite, its Gibbs free energy of formation can be calculated by the equation:

$$\Delta G°_f = \Delta H°_f - T\,.\,\Delta S°_f \quad (8)$$

where $\Delta S°_f$ is the entropy of formation from the elements. Application of Eqn. (8) leads to the value $\Delta G°_f = -1818.8 \pm 6.4$ kJ.mol^{-1}. The thermodynamic data that we recommend for yavapaiite, in view of this work, are presented in Table 2.

Based on measured data for yavapaiite and data from the literature for jarosite, we calculate the stability field of jarosite in Earth and Mars environments. The presence of sulfates on the Martian surface have been inferred from spectroscopic data (Pollack et al., 1990; Blaney and McCord, 1995), lander surface analysis or from image analysis (Thomas et al., 1999). Also presence of water has been confirmed by several researchers (Malin and Edgett, 2000; Mustard et al., 2001; Mitrofanov et al., 2003; Titus et al., 2003). Recently the Mars exploration rover Opportunity identified the presence of jarosite, on the basis of Mossbauer spectrometry (Klingelhöfer, 2004). We therefore calculate the stability field of jarosite vs. yavapaiite on the Martian surface.

The yavapaiite heat capacity was estimated from thermodynamic data on $KAl(SO_4)_2$, $Fe_2(SO_4)_3$, $Al_2(SO_4)_3$, hematite, and corundum using the method of Helgeson et al. (1978) for the temperature range 100–973 K. The heat capacity data for jarosite were computed using data from Drouet and Navrotsky (2003) and Majzlan et al. (2004).

Thermodynamic calculations show that under low total atmospheric pressure (6 mbar) on Mars (Kliore et al., 1965) where the partial pressure of the H_2O is ~0.0025 mbar), the equilibrium decomposition of jarosite to yavapaiite, hematite and water vapor (Eqn. 1) takes place at + 18°C. The highest temperature measured at the Mars surface was + 17°C and the average surface temperature at the equator is around −58°C (Kieffer et al., 1977). Thus it is reasonable that jarosite persists in deposits on the Martian surface since it is within its thermodynamic stability field.

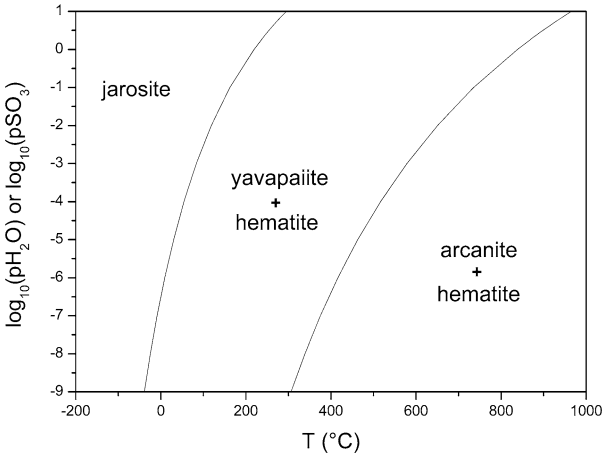

Fig. 5. Region of thermal stability (log of partial pressure (atm) of H_2O or SO_3) of yavapiite in a system with jarosite composition. At low temperature, stability is limited by formation of the hydrated phase, jarosite, and depends on pH_2O. At high temperature, stability is limited by decomposition to $K_2SO_4 + Fe_2O_3 + SO_3$ and depends on pSO_3. Stability fields are labeled by the solid phases present. The temperature uncertainty is ± 7°C.

If we consider just equilibrium thermal decomposition, then jarosite will be stabile at the surface of Mars. Experimental simulation of the photodecomposition of carbonates and sulfates on Mars was performed by Mukhin et al. (1996). They found that solar ultraviolet radiation is able to decompose sulfates and raise the temperature of the minerals by about 25°C. Considering the effect of such temperature increase, and of the solar ultraviolet radiation, we conclude that jarosite might decompose slightly on the surface of Mars but a thin layer of decomposition products (iron oxide) on the jarosite surface would probably protect the jarosite from further decomposition. Thus the relatively massive jarosite deposits inferred from the current rover explorations are thermodynamically reasonable. They persist to the present day because they are thermodynamically stable, but their initial formation presumably required wetter conditions for effective mass transport and crystallization.

At the Earth's surface, thermodynamic calculations show that jarosite starts to decompose (Eqn. 1) at ~219 ± 2°C (Fig. 5). The uncertainty of this decomposition temperature was calculated using the propagation of errors in general form of Eqn. (8) based on the uncertainty of the thermodynamic data used. Drouet and Navrotsky (2003) mention the first endothermic peak in the thermal analysis of the jarosite at 220°C, and they attribute it to loss of H_2O molecules. The loss of H_2O was also observed by Kubisz (1971). The X-ray diffraction pattern of jarosite heated to 280°C indicates the presence of trace amount of $K_3Fe(SO_4)_3$ (Drouet and Navrotsky, 2003). This indicates

that jarosite is not stable at this temperature and is consistent with the new thermochemical data.

Figure 5 shows the equilibrium stability field of yavapaiite, calculated from the thermochemical data. A system with the initial composition of jarosite is considered. At low temperature yavapaiite stability is limited by the formation of jarosite (reverse of Eqn. 1). As discussed above, the temperature of decomposition depends on pH_2O. In a closed or partially closed system, the generated water pressure allows the two phase assemblage to coexist at a given temperature. In an open system, decomposition occurs continuously as water is evolved. The high temperature decomposition of yavapaiite generates SO_3 (as to be more exact, a mixture of SO_2, SO_3 and O_2). The decomposition temperature will then depend on the partial pressure of these gases (shown, for simplicity, as SO_3 in the figure). Once again, in an open system, gas evolution will constantly drive the system toward decomposition. The temperature at which decomposition is just detected will depend both on the sensitivity of the detection method and on the extent to which some sulfur gases are retained in contact whit the sample (sample and containers geometry, gas flow rates, etc.).

We conclude that these thermochemical studies enable one to map, and the regions of stability of jarosite and yavapaiite, and to predict this stability under terrestrial and Martian conditions.

Acknowledgments—This work was supported by the U.S. Department of Energy grant DEFG0397SF14749. We would like to thank to D.A. Sverjensky and anonymous reviewers for their helpful comments and suggestions which improve the quality of this paper.

Associate editor: D. Sverjensky

REFERENCES

Anthony J. W., McLean W. J. and Laughon R. B. (1972) The crystal structure of yavapaiite: a discussion. *Am. Mineral.* **57,** 1546–1549.

Arkhipenko D. K., Deviatkina E. T. and Palchik H. A. (1987) Kristallokhimicheskiye osobennosti sinteticheskikh yarozitov (in Russian). *Trudy Inst. Geolog. I Geofiz.* **653,** 31–70.

Arno M. (1984) Iron oxide from jarosite and similar compounds. Patent no. DD 215999, Germany, 6.

Blaney D. L. and McCord T. B. (1995) Indications of sulfate minerals in the Martian soil from Earth-based spectroscopy. *J. Geophys. Res.* **100** (**E7**), 14,433–14,442.

Bramwell S. T., Carling S. G., Harding C. J., Harris K. D. M., Kariuki B. M., Nixon L. and Parkin I. P. (1996) The anhydrous alums as model triangular-lattice magnets. *J. Phys. Condens. Matter* L123–L129.

Burns R. G. Ferric sulfates on Mars. (1987) *J. Geophys. Res.* **92,** E570-E574.

Drouet C. and Navrotsky A. (2003) Synthesis, characterisation and thermochemistry of K-Na-H_3O jarosites. *Geochim. Cosmochim. Acta* 2063–2076.

Effenberger H., Pertlik F. and Zemann J. (1986) Refinement of the crystal structure of krausite: a mineral with an interpolyhedral oxygen-oxygen contact shorter than the hydrogen bond. *Am. Mineral.* **71,** 202–205.

Florencia M., Zavalía M. and Galliski M. A. (1995) Goldichite of fumarolic origin from the Santa Bárbara Mine, Jujuy, northwestern Argentina. *Can. Mineral.* **33,** 1059–1062.

Foshag W. F. (1931) Krausite, a new sulfate from California. *Am. Mineral.* **16,** 352–360.

Furtado N. C., Taft C. A. and Cassedane J. O. (1989) Oxidation of potassium dithioferrate and consequent formation of the mineral yavapaiite. *J. Mat. Sci.* **24** (*8*), 2751–2755.

Giester G. (1993) Crystal structure of the Yavapaiite type compound. *Mineral. Petrol.* **48,** 227–233.

Giester G. (1995) Crystal structure of $KMn^{3+}[SeO_4]_2$—a triclinic distorted member of the Yavapaiite family. *Mineral. Petrol.* **53,** 165–171.

Graeber E. J., Morosin B. and Rosenzweig A. (1965) The crystal structure of krausite, $KFe(SO_4)_2 \cdot H_2O$. *Am. Mineral.* **50,** 1929–1936.

Graeber E. J. and Rosenzweig A. (1971) The crystal structure of yavapaiite, $KFe(SO_4)_2$ and goldichite, $KFe(SO_4)_2 \cdot 4H_2O$. *Am. Mineral.* **56,** 1917–1933.

Helgeson H. C., Delany J. and Bird D. K. (1978) Summary and critique of the thermodynamic properties of rock-forming minerals. *Am. J. Sci.* **278A**, 1–229.

Hutton O. C. (1959) Yavapaiite, an anhydrous potassium, ferric sulphate from Jerome, Arizona. *Am. Mineral.* **44,** 1105–1114.

Kieffer H. H., Martin T. Z., Peterfreund A. R., Jakosky B. M., Miner E. D. and Palluconi F. D. (1977) Thermal and albedo mapping of Mars during the Viking primary mission. *J. Geophys. Res.* **82,** 4249–4291.

Klingelhöfer G., Morris R. V., Bernhardt B., Schröeder C., Rodionov D. S., de Souza P. A. J., Yen A., Gellert R., Evlanov E. N., Zubkov B., Foh J., Bonnes U., Kankeleit E., Gütlich P., Ming D. W., Renz F., Wdowiak T., Squyres S. W. and Arvidson R. E. (2004) Jarosite and hematite at Meridiani Planum from Opportunity's mössbauer spectrometer. *Science* **306** (5702), 1740–1745.

Kliore A. J., Cain D. L., Levy G. S., Eshleman V. R., Fijeldbo G. and Drake F. D. (1965) Occultation experiment: Results of the first direct measurement of Mars' atmosphere and ionosphere. *Science* **149,** 1243–1248.

Kubisz J. (1971) Studies on synthetic alkali-hydronium jarosites II: thermal investigations. *Mineral. Polon.* **2,** 51–59.

Kulp J. L. and Adler H. H. (1950) Thermal study of jarosite. *Am. J. Sci.* **248,** 475–487.

Leclaire A., Borel M. M., Chardon J. and Raveau B. (1995) A Mo(IV) monophosphate, $BaMo(PO_4)_2$, with the yavapaiite layer structure. *J. Sol. Stat. Chem.* **116,** 364–368.

Majzlan J., Navrotsky A. and Neil J. M. (2002) Energetics of anhydrite, barite, celestine and anglesite: A high-temperature and differential scanning calorimetry study. *Geochim. Cosmochim. Acta* **66** (*10*), 1839–1850.

Majzlan J., Navrotsky A., Stevens R., Boerio-Goates J., Woodfield B. F., Burns P. C., Crawford M. K., and Amos T. G. (2004) Thermodynamic properties, low-temperature heat capacity anomalies and single crystal X-ray refinement of hydronium jarosite, $(H_3O)Fe_3(OH)_6(SO_4)_2$. *Phys. Chem Min.*, **31** (8), 518–531.

Malin M. C. and Edgett K. S. (2000) Evidence for recent groundwater seepage and surface runoff on Mars. *Science* **288,** 2330–2335.

Materials Data Inc. (2001) Jade 6.1 [Computer program]. Livermore, CA.

Miao C. R. and Torardi C. C. (2000) A new high-efficiency UV-emitting X-ray phosphor, $BaHf_{1-x}Zr_x(PO_4)_2$. *J. Sol. Stat. Chem.* **155,** 229–232.

Mitrofanov I. G., Zuber M. T., Litvak M. L., Boynton W. V., Smith D. E., Drake D., Hamara D., Kozyrev A. S., Sanin A. B., Shinohara C., Saunders R. S. and Tretyakov V. (2003) CO_2 snow depth and subsurface water-ice abundance in the Northern hemisphere of Mars. *Science* **300,** 2081–2084.

Morris R. V. and Golden D. C. (1998) Goldenrod pigments and the occurrence of hematite and possibly goethite in the Olympus-Amazonis region of Mars. *Icarus* **134** (*1*), 1–10.

Mukhin L. M., Koscheev A. P., Dikov Y. P., Huth J. and Wänke H. (1996) Experimental simulations of the photodecomposition of carbonates and sulphates on Mars. *Nature* **379,** 141–143.

Mustard J. F., Cooper C. D. and Rifkin M. K. (2001) Evidence for recent climate change on Mars from the identification of youthful near-surface ground ice. *Nature* **412,** 411–414.

Navrotsky A. (1977) Progress and new directions in high temperature calorimetry. *Phys. Chem. Min.* **2,** 89–104.

Navrotsky A. (1997) Progress and new directions in high temperature calorimetry revisited. *Phys. Chem. Min.* **24,** 222–241.

Navrotsky A., Rapp R. P., Smelik E., Burnley P., Circone S., Chai L., Bose K. and Westrich H. R. (1994) The behavior of H_2O and CO_2 in high-temperature lead borate solution calorimetry of volatile-bearing phases. *Am. Mineral.* **79,** 1099–1109.

Pollack J. B., Roush T., Witterborn F., Bregman J., Wooden D., Stoker C., Toon O. B., Rank D., Dalton B. and Freedman R. (1990) Thermal emission spectra of Mars (5.4–10.5 μm): evidence for sulfates, carbonates and hydrates. *J. Geophys. Res.* **95** (**B9**), 14,595–14,627.

Robie R. A. and Hemingway B. S. (1995) Thermodynamic properties of minerals and related substances at 298.15 K and 1 Bar (10^5 Pascals) pressure and at higher temperatures. U.S.G.S. Bulletin 2131, 461 pp.

Rosenzweig A. and Gross E. B. (1955) Goldichite, a new hydrous potassium ferric sulfate from the San Rafael swell, Utah. *Am. Mineral.* **40,** 469–480.

Smith B. (1999) Inorganic compounds. In *Infrared spectral interpretation. A systematic approach*, pp. 165–175. CRC Press.

Thomas P. C., Malin M. C., Carr M. H., Danielson G. E., Davies M. E., Hartmann W. K., Ingersoll A. P., James P. B., McEwen A. S., Soderblom L. A. and Veverka J. (1999) Bright dunes on Mars. *Nature* **397,** 592–594.

Titus T. N., Kieffer H. H. and Christensen P. R. (2003) Exposed water ice discovered near South Pole of Mars. *Science* **299,** 1048–1051.

Volchanova E., Kalcheva A. and Shumlyanskii V. (1974) Minerals in the oxidation zone of the hydrothermal mineralization in the Mount Kozhukh. *Spis. Bulgarsk. Geolog. Druz.* **35** (*3*), 334–338.